IEEE Access
Multidisciplinary | Rapid Review | Open Access Journal

Received June 11, 2021, accepted June 27, 2021, date of publication June 30, 2021, date of current version July 8, 2021.

Digital Object Identifier 10.1109/ACCESS.2021.3093719

Distributed GM-CPHD Filter Based on Generalized Inverse Covariance Intersection

WOO JUNG PARK[1] AND CHAN GOOK PARK[2], (Member, IEEE)
[1]Department of Mechanical and Aerospace Engineering / Automation and System Research Institute, Seoul National University, Seoul 08826, Republic of Korea
[2]Department of Mechanical and Aerospace Engineering / Institute of Advanced Aerospace Technology, Seoul National University, Seoul 08826, Republic of Korea

Corresponding author: Chan Gook Park (chanpark@snu.ac.kr)

This work was supported by the Unmanned Vehicles Core Technology Research and Development Program through the National Research Foundation of Korea (NRF), Unmanned Vehicle Advanced Research Center (UVARC) funded by the Ministry of Science and Information and Communications Technology (ICT), South Korea, under Grant NRF-2020M3C1C1A01086408.

ABSTRACT In this paper, we propose a distributed Gaussian mixture cardinalized probability hypothesis density (GM-CPHD) filter based on generalized inverse covariance intersection that fuses multiple node information effectively for multi-target tracking applications. Covariance intersection (CI) is a well-known fusion method that produces a conservative estimate of the joint covariance regardless of the actual correlation between the different nodes. Inverse covariance intersection (ICI) is the updated version to obtain fusion results that guarantee consistency and less conservative than CI. However, the ICI is not extended to multi-sensor multi-target tracking system yet. Since the ICI formula can be re-structured as naïve fusion with covariance inflation in Gaussian pdf, this method was applied to the GM-CPHD with generalization. The formula for random finite set (RFS) fusion was derived in the same way as the conventional generalized covariance intersection (GCI) based fusion. The simulation results for multi-target tracking show that the proposed algorithm has smaller optimal sub-pattern assignment (OSPA) errors than naïve fusion and the GCI-based fusions.

INDEX TERMS Multi-target tracking, GM-CPHD filter, inverse covariance intersection, covariance inflation.

I. INTRODUCTION

Multi-target tracking (MTT) is the research that tracks multiple targets with their states, such as position and velocity. MTT problem can be solved by finite set statistics (FISST) without complicated data association, which is based on a random finite set (RFS) [1]. The probability hypothesis density (PHD) filter is the first RFS filter that propagates the filter's first-order moment [2]. To improve the cardinality estimation performance of the PHD filter, a cardinalized PHD (CPHD) filter is introduced, which jointly estimates intensity and cardinality distribution [3]. Unlike the suboptimal filters like PHD and CPHD, the first optimal multi-target Bayesian filter is proposed using labeled multi-Bernoulli RFS, which is called δ-generalized labeled multi-Bernoulli filter (δ-GLMB) [4]. In addition, labeled multi-Bernoulli (LMB) and Gibbs sampling based LMB filters are proposed to reduce the computation complexity of the δ-GLMB filter with some approximations [5]. These RFS-based filters are widely used in surveillance systems, autonomous vehicles, and computer vision applications [6]–[9].

Recently, single-sensor multi-target RFS filters are extended to multi-sensor multi-target (MS-MT) RFS filters to improve tracking accuracy and robustness. Multi-sensor architecture is mainly divided into a centralized system and distributed system. Centralized system is generally known to provide an optimal solution, and it is applied to many RFS filters, which result in centralized MS-CPHD [10], MS-MeMBer [11], and MS-GLMB [12]. However, a centralized MS-MT system needs partitioning of the sensor measurements into disjoint subsets, which is computationally intractable [13]. On the other hand, distributed systems have low computational load and conservative to the unknown correlation between nodes [13]–[16]. Also, it is relatively easy to manage the tracks and tolerant to the fault of the

The associate editor coordinating the review of this manuscript and approving it for publication was Rui-Jun Yan.

sensor. Especially, average consensus drew attention in the distributed fusion research area, which is flexible and scalable [13], [17]–[20]. The linear arithmetic average (AA) and the log-linear geometric average (GA) are widely used among average consensus. According to the previous works, AA performs better than GA when the detection probability is low, and targets are close [17], [21]. On the opposite, GA performs better than AA in high clutter density and high false alarm rate.

After the research on centralized MS-MT system, distributed MS-MT system with Gaussian mixture (GM) implementation was proposed, including average consensus-based GM-CPHD [22], [23] and GM-MB [24], [25]. In particular, GA with optimized weights is called generalized covariance intersection (GCI) [26], [27], which is a generalization version of covariance intersection (CI) [28] to fuse non-Gaussian pdf. GCI has various names, such as Chernoff fusion, geometric mean density, and Kullack-Leibler average [29]. The aforementioned GCI-based researches [22]–[25] use pseudo-Chernoff fusion [30] for GM implementation. To approximate a non-integer power of a Gaussian mixture more accurately, sigma-point Chernoff fusion was developed [29]. A partial consensus approach for distributed GM-PHD, which exchanges only highly-weighted Gaussian components, was proposed [19].

CI is a well-known fusion method that produces a conservative estimate of the joint covariance regardless of the actual correlation between the different nodes. Ellipsoidal intersection (EI) [31] was proposed to achieve a less conservative result than CI, but it does not guarantee consistency [32]. To obtain a fusion result that guarantees consistency and less conservative than CI, inverse covariance intersection (ICI) was proposed [32]. It was proved that the covariance of the ICI is smaller than CI [32], [33]. As CI has been extended to GCI, both the EI and ICI are also extended to a generalized ellipsoidal intersection [34] and nonlinear inverse covariance intersection (NICI) [35] to fuse arbitrary pdfs, respectively. To unify the terms, we will call the NICI as generalized inverse covariance intersection (GICI). Besides, to apply the generalized fusion to MS-MT, fusion formulation on RFS must be defined which was done in CI [27]. However, EI and ICI are not extended to the MS-MT system yet.

In this paper, we propose a distributed GM-CPHD filter based on GICI. To extend GICI to the MS-MT system, we suggest a new approach to GICI, which is different from the conventional GICI [35]. The suggested method uses the covariance inflation technique to naïve fusion, which will be discussed in the next section. Notice that it is based on covariance inflation of the CI fusion without feedback which is different from the information sharing of the federated Kalman filter [36], [37]. By this approach, we can formulate GICI based GM-CPHD filter.

This paper is organized as follows. In section II, the MS-CPHD filter and GCI fusion are explained briefly. The proposed GICI based GM-CPHD filter is described in section III. The simulation results are presented in section IV, and the conclusion is written in section V.

II. BACKGROUND

When tracking multi-target, which estimates both the state vectors and the cardinality, RFS-based trackers are preferred to the multiple independent single-target trackers since they jointly solve both problems [22]. In addition, a mathematical tool called FISST is widely used to formulate multi-target tracking using Bayesian filtering problems in the RFS framework. This section reviews the background of FISST [1]. Also, based on FISST, CPHD filter [3], and GCI fusion for GM-CPHD [27] are reviewed briefly.

A. FINITE SET STATISTICS

A multi-object density function $f(\mathbf{X})$ is a real-valued function of an RFS $\mathbf{X} = \{\mathbf{x}_1, \cdots, \mathbf{x}_n\}$, and a multi-object density function characterizes the RFS. The set integral of the multi-object density function is defined as [1],

$$\int f(\mathbf{X})\delta\mathbf{X} \triangleq f(\phi) + \sum_{n=1}^{\infty} \frac{1}{n!} \int f(\{\mathbf{x}_1, \cdots, \mathbf{x}_n\})\, d\,\mathbf{x}_1 \cdots d\mathbf{x}_n. \tag{1}$$

Besides, probability generating functional (PGFL) $G[h]$ and probability hypothesis density $D(\mathbf{x})$ are defined as

$$G[h] \triangleq \int f(\mathbf{X}) h^X \delta\mathbf{X}, \tag{2}$$

$$h^X \triangleq \prod_{\mathbf{x}\in\mathbf{X}} h(\mathbf{x}), \tag{3}$$

$$D(\mathbf{x}) \triangleq \frac{\delta}{\delta\mathbf{x}} G[h]\Big|_{h=1}, \tag{4}$$

where h is the test function. PGFL uniquely determines the multi-object density, and it can be interpreted as one of the transforms to solve problems in MTT easily. Otherwise, PHD is the first-order moment of multi-object density. By integrating the PHD function in some regions, we can obtain the expected number of targets in the region.

B. CPHD FILTER

CPHD filter is defined by the multi-object distribution with an independent, identically distributed (i.i.d.) process. Let $p(n)$ be the cardinality distribution of the point process $|\mathbf{X}| = n$, then [27]

$$f(\mathbf{X}) \triangleq n! \cdot p(n) \cdot f(\mathbf{x}_1) \cdots f(\mathbf{x}_n). \tag{5}$$

The PGFL of an i.i.d. process is

$$G[h] = \sum_{n=0}^{\infty} p(n) \left(\int h(u) \cdot f(u) du \right)^n. \tag{6}$$

The intensity function of an i.i.d. process is found with

$$D(\mathbf{x}) = \frac{\delta}{\delta\mathbf{x}} G[h]\Big|_{h=1} = f(\mathbf{x}) \sum_{n=1}^{\infty} n \cdot p(n). \tag{7}$$

which is the product of the single-object density $f(x)$, and the expected number of objects $\sum_{n=1}^{\infty} n \cdot p(n)$.

C. GCI FUSION FOR CPHD FILTER

Assume two Gaussian distributions $\mathbf{x} \sim N(\hat{\mathbf{x}}_a, \hat{\mathbf{P}}_a)$ and $\mathbf{x} \sim N(\hat{\mathbf{x}}_b, \hat{\mathbf{P}}_b)$, where subscript a and b are the node numbers. Then, fusion by CI can be applied as

$$N_{\hat{\mathbf{P}}_\omega}(\mathbf{x}-\hat{\mathbf{x}}_\omega) = \frac{N_{\hat{\mathbf{P}}_a/\omega}(\mathbf{x}-\hat{\mathbf{x}}_a)N_{\hat{\mathbf{P}}_b/(1-\omega)}(\mathbf{x}-\hat{\mathbf{x}}_b)}{\int N_{\hat{\mathbf{P}}_a/\omega}(\mathbf{x}-\hat{\mathbf{x}}_a)N_{\hat{\mathbf{P}}_b/(1-\omega)}(\mathbf{x}-\hat{\mathbf{x}}_b)d\mathbf{x}} = \frac{N_{\hat{\mathbf{P}}_a}(\mathbf{x}-\hat{\mathbf{x}}_a)^\omega N_{\hat{\mathbf{P}}_b}(\mathbf{x}-\hat{\mathbf{x}}_b)^{1-\omega}}{\int N_{\hat{\mathbf{P}}_a}(\mathbf{x}-\hat{\mathbf{x}}_a)^\omega N_{\hat{\mathbf{P}}_b}(\mathbf{x}-\hat{\mathbf{x}}_b)^{1-\omega}d\mathbf{x}}, \tag{8}$$

where $\omega \in (0, 1)$ is a weight.

GCI is the generalized rule of CI formula (8) to fuse multi-object densities with arbitrary density, which is also known for Chernoff fusion,

$$f_\omega(\mathbf{x}|\mathbf{Z}_a^k, \mathbf{Z}_b^k) \triangleq \frac{f_a(\ \mathbf{x}|\mathbf{Z}_a^k)^\omega f_b(\mathbf{x}|\mathbf{Z}_b^k)^{1-\omega}}{\int f_a(\mathbf{x}|\mathbf{Z}_a^k)^\omega f_b(\ \mathbf{x}|\mathbf{Z}_b^k)^{1-\omega}d\mathbf{x}}. \tag{9}$$

In reverse, CI is a special case of GCI when distributions to be fused are Gaussian [38]. GCI is proved to minimize the Kullbeck-Leibler divergence(KLD) [22],

$$f_{KLA}(\mathbf{X}) = \arg\inf_f \sum_i \omega_i \mathbf{D}_{KL}\left(f||f^i\right) = \frac{\prod_i \left[f^i(\mathbf{X})\right]^{\omega_i}}{\int \prod_i \left[f^i(\mathbf{X})\right]^{\omega_i} d\ \mathbf{X}}, \tag{10}$$

$$\mathbf{D}_{KL}(p_i||p_j) \int p_i \triangleq (\mathbf{X}) \log \frac{p_i(\mathbf{X})}{p_j(\mathbf{X})} d\mathbf{X}. \tag{11}$$

Now, consider the local multi-object densities of the CPHD filter that should be fused are

$$f_a(\mathbf{X}) = n! \cdot p_a\,(n) \prod_{\mathbf{x}\in\mathbf{X}} s_a(\mathbf{x}),$$
$$f_b(\mathbf{X}) = n! \cdot p_b\,(n) \prod_{\mathbf{x}\in\mathbf{X}} s_b(\mathbf{x}), \tag{12}$$

where $s(\mathbf{x})$ means local density.

By applying GCI, the results of the fused multi-object density and cardinality are [27],

$$\bar{s}(\mathbf{x}) = \frac{s_a^\omega(\mathbf{x})s_b^{1-\omega}(\ \mathbf{x})}{\int s_a^\omega(\mathbf{x})s_b^{1-\omega}(\mathbf{x})d\ \mathbf{x}}, \tag{13}$$

$$\bar{p}(n) = \frac{p_a^\omega(n)p_b^{1-\omega}(n)\left(\int s_a^\omega(\ \mathbf{x})s_b^{1-\omega}(\mathbf{x})d\mathbf{x}\right)^n}{\sum_{m=0}^{\infty} p_a^\omega(m)p_b^{1-\omega}(m)\left(\int s_a^\omega(\mathbf{x})s_b^{1-\omega}(\ \mathbf{x})d\mathbf{x}\right)^m}. \tag{14}$$

D. GAUSSIAN MIXTURE IMPLEMENTATION

For Gaussian mixture form of the local density

$$s_a(\mathbf{x}) = \sum_{j=1}^{N_G^a} \alpha_j^{(a)} N(\hat{\mathbf{x}}_j^{(a)}, \mathbf{P}_j^{(a)}), \tag{15}$$

If the Gaussian components are well-separated as

$$\left(\hat{\mathbf{x}}_i - \hat{\mathbf{x}}_j\right)^T \mathbf{P}_i^{-1} \left(\hat{\mathbf{x}}_i - \hat{\mathbf{x}}_j\right) \gg 1, \tag{16}$$
$$\left(\hat{\mathbf{x}}_i - \hat{\mathbf{x}}_j\right)^T \mathbf{P}_j^{-1} \left(\hat{\mathbf{x}}_i - \hat{\mathbf{x}}_j\right) \gg 1. \tag{17}$$

Following approximation can be applied

$$s_a^\omega(\mathbf{x}) = \left[\sum_{j=1}^{N_G^a} \alpha_j^{(a)} N(\hat{\mathbf{x}}_j^{(a)}, \mathbf{P}_j^{(a)})\right]^\omega \cong \sum_{j=1}^{N_G^{(a)}} \left[\alpha_j^{(a)} N(\hat{\mathbf{x}}_j^{(a)}, \mathbf{P}_j^{(a)})\right]^\omega = \sum_{j=1}^{N_G^a} (\alpha_j^{(a)})^\omega \kappa(\omega, \mathbf{P}_j^{(a)}) N(\hat{\mathbf{x}}_j^{(a)}, \frac{\mathbf{P}_j^{(a)}}{\omega}), \tag{18}$$

where $\kappa(\omega, \mathbf{P}) \triangleq \omega^{-\frac{n}{2}} \det(2\pi\mathbf{P})^{\frac{1-\omega}{2}}$. The approximation is from pseudo-Chernoff fusion [30] and is widely used in GM-GCI approaches.

By using (18), fused multi-object density (13) can be obtained in closed form,

$$\bar{s}_{\mathbf{GCI}}(\mathbf{x}) = \frac{s_a^\omega(\mathbf{x})s_b^{1-\omega}(\mathbf{x})}{\int s_a^\omega(\mathbf{x})s_b^{1-\omega}(\mathbf{x})d\ \mathbf{x}} = \frac{\sum_{i=1}^{N_G^a}\sum_{j=1}^{N_G^b} \alpha_{ij}^{(ab)} N(\hat{\mathbf{x}}_{ij}^{(ab)}, \mathbf{P}_{ij}^{(ab)})}{\sum_{i=1}^{N_G^a}\sum_{j=1}^{N_G^b} \alpha_{ij}^{(ab)}}, \tag{19}$$

$$\mathbf{P}_{ij}^{(ab)} = \left[\omega\left(\mathbf{P}_i^{(a)}\right)^{-1} + (1-\omega)\left(\mathbf{P}_j^{(b)}\right)^{-1}\right]^{-1}, \tag{20}$$

$$\hat{\mathbf{x}}_{ij}^{(ab)} = \mathbf{P}_{ij}^{(ab)}\left[\omega\left(\mathbf{P}_i^{(a)}\right)^{-1}\hat{\mathbf{x}}_i^{(a)} + (1-\omega)\left(\mathbf{P}_j^{(b)}\right)^{-1}\hat{\mathbf{x}}_j^{(b)}\right], \tag{21}$$

$$\alpha_{ij}^{(ab)} = \left(\alpha_i^{(a)}\right)^\omega \left(\alpha_j^{(b)}\right)^{1-\omega} \kappa\left(\omega,\ \mathbf{P}_i^{(a)}\right)\kappa\left(1-\omega,\ \mathbf{P}_j^{(b)}\right) \cdot N\left(\hat{\mathbf{x}}_i^{(a)} - \hat{\mathbf{x}}_j^{(b)};\ 0,\ \frac{\mathbf{P}_i^{(a)}}{\omega} + \frac{\mathbf{P}_j^{(b)}}{1-\omega}\right). \tag{22}$$

III. DISTRIBUTED FUSION BASED ON GENERALIZED NAÏVE FUSION WITH COVARIANCE INFLATION

To apply ICI to multi-object density fusion, naïve fusion with covariance inflation is proposed in this section.

A. THREE COMMON DISTRIBUTED FUSION RULES

Let us consider the fusion of two nodes $\mathbf{x} \sim N(\mathbf{x_A},\ \mathbf{P_A})$, $\mathbf{x} \sim N(\mathbf{x_B},\ \mathbf{P_B})$ which follow Gaussian distribution. Since EI is proven to be inconsistent [26], it is not dealt with in this paper.

Firstly, naïve fusion [39], which is optimal when there is no correlation,

$$\mathbf{x}_{naive} = \mathbf{P}_{naive}(\mathbf{P_A}^{-1}\ \mathbf{x_A} + \mathbf{P_B}^{-1}\mathbf{x_B}), \tag{23}$$
$$\mathbf{P}_{naive} = \left(\mathbf{P_A}^{-1} + \mathbf{P}^{-1}{}_{\mathbf{B}}\right)^{-1}. \tag{24}$$

Meanwhile, CI is the fusion rule that keeps consistency under unknown correlation of the nodes

$$\begin{aligned}\mathbf{x_{CI}} &= \mathbf{P_{CI}}(\omega_{\mathbf{CI}}\mathbf{P_A}^{-1}\mathbf{x_A} + (1-\omega_{\mathbf{CI}})\mathbf{P_B}^{-1}\mathbf{x_B}) \\ &= \mathbf{P_{CI}}(\mathbf{P}_{\mathbf{A,CI}}^{-1}\ \mathbf{x_A} + \mathbf{P}_{\mathbf{B,CI}}^{-1}\ \mathbf{x_B}), \qquad (25)\\ \mathbf{P_{CI}} &= \left(\omega_{\mathbf{CI}}\mathbf{P_A}^{-1} + (1-\omega_{\mathbf{CI}})\mathbf{P_B}^{-1}\right)^{-1} \\ &= \left(\mathbf{P}_{\mathbf{A,CI}}^{-1} + \mathbf{P}_{\mathbf{B},\mathbf{CI}}^{-1}\right)^{-1}, \qquad (26)\\ \mathbf{P}_{\mathbf{A,CI}}^{-1} &\triangleq \omega_{\mathbf{CI}}\ \mathbf{P_A}^{-1}, \qquad (27)\\ \mathbf{P}_{\mathbf{B,CI}}^{-1} &\triangleq (1-\omega_{\mathbf{CI}})\ \mathbf{P_B}^{-1}, \qquad (28)\end{aligned}$$

where $\omega_{\mathbf{CI}} \in (0,1)$ is a weight and often obtained by $\min_{\omega}(\det(\mathbf{P_{CI}}))$ or $\min_{\omega}(trace(\mathbf{P_{CI}}))$. Since the optimization procedure for calculating $\omega_{\mathbf{CI}}$ is computationally intensive, $\omega_{\mathbf{CI}}$ can be obtained by various fast covariance intersection methods which provide a closed-form solution without optimization [40]–[43].

The thing to note (25-28) is, by changing covariance $\mathbf{P_A}$ and $\mathbf{P_B}$ to $\mathbf{P}_{\mathbf{A,CI}}$ and $\mathbf{P}_{\mathbf{B,CI}}$ respectively, the CI formula is transformed to naïve fusion.

Recently, ICI is proposed to obtain fusion results, which guarantee consistency and less conservative than CI [32]. It is proved that the covariance of the ICI is smaller than CI [32], [33]. The ICI formula can be written as [32],

$$\begin{aligned}\mathbf{x_{ICI}} &= \mathbf{K_{ICI}}\mathbf{x}_{\mathbf{A}} + \mathbf{L_{ICI}}\mathbf{x_B}, \qquad (29)\\ \mathbf{P_{ICI}^{-1}} &= \mathbf{P}_{\mathbf{A,ICI}}^{-1} + \mathbf{P}_{\mathbf{B,ICI}}^{-1} - (\omega_{\mathbf{ICI}}\,\mathbf{P_A} \\ &\quad + (1-\omega_{\mathbf{ICI}})\mathbf{P_B})^{-1}, \qquad (30)\\ \mathbf{K_{ICI}} &= \mathbf{P_{ICI}}(\mathbf{P_A}^{-1} - \omega_{\mathbf{ICI}}(\omega_{\mathbf{ICI}}\mathbf{P}_{\mathbf{A}} \\ &\quad + (1-\omega_{\mathbf{ICI}})\mathbf{P}_B)^{-1}), \qquad (31)\\ \mathbf{L_{ICI}} &= \mathbf{P_{ICI}}(\mathbf{P_B}^{-1} - (1-\omega_{\mathbf{ICI}})(\omega_{\mathbf{ICI}}\mathbf{P}_{\mathbf{A}} \\ &\quad + (1-\omega_{\mathbf{ICI}})\mathbf{P}_B)^{-1}). \qquad (32)\end{aligned}$$

B. INVERSE COVARIANCE INTERSECTION FROM THE PERSPECTIVE OF COVARIANCE INFLATION

To apply ICI to the MS-MT, we changed the structure of the original ICI formula (29)-(32) as,

$$\begin{aligned}\mathbf{x_{ICI}} &= \mathbf{P_{ICI}}(\mathbf{P}_{\mathbf{A,ICI}}^{-1}\mathbf{x_A} + \mathbf{P}_{\mathbf{B,\,ICI}}^{-1}\mathbf{x_B}), \qquad (33)\\ \mathbf{P_{ICI}} &= \left(\mathbf{P_A}^{-1} + \mathbf{P_B}^{-1} - (\omega_{\mathbf{ICI}}\mathbf{P_A} + (1-\omega_{\mathbf{ICI}})\mathbf{P_B})^{-1}\right)^{-1} \\ &= \left(\mathbf{P}_{\mathbf{A,ICI}}^{-1} + \mathbf{P}_{\mathbf{B,ICI}}^{-1}\right)^{-1}, \qquad (34)\\ \mathbf{P}_{\mathbf{A,ICI}}^{-1} &\triangleq \mathbf{P_A}^{-1} - \omega_{\mathbf{ICI}}(\omega_{\mathbf{ICI}}\mathbf{P}_{\mathbf{A}} + (1-\omega_{\mathbf{ICI}})\mathbf{P}_B)^{-1}, \qquad (35)\\ \mathbf{P}_{\mathbf{B,ICI}}^{-1} &\triangleq \mathbf{P_B}^{-1} - (1-\omega_{\mathbf{ICI}})(\omega_{\mathbf{ICI}}\mathbf{P}_{\mathbf{A}} + (1-\omega_{\mathbf{ICI}})\mathbf{P}_B)^{-1}, \qquad (36)\end{aligned}$$

where $\omega_{\mathbf{ICI}} \in (0,1)$ is a weight and obtained by $\min_{\omega}(\det(\mathbf{P_{ICI}}))$ or $\min_{\omega}(trace(\mathbf{P_{ICI}}))$. In the extreme case $\omega_{\mathbf{ICI}} = 0$, it becomes $\mathbf{x_{ICI}} = \mathbf{x_A}, \mathbf{P_{ICI}} = \mathbf{P_A}$. In the opposite case $\omega_{\mathbf{ICI}} = 1$, it becomes $\mathbf{x_{ICI}} = \mathbf{x}_{\mathbf{B}}, \mathbf{P_{ICI}} = \mathbf{P}_{\mathbf{B}}$. Since they are not fusion and only result from one node, we defined $\omega_{\mathbf{ICI}}$ in the open interval $(0,1)$.

As shown in (35-36), the ICI formula can also be transformed to naïve fusion by changing the nodes' covariance.

Since $\omega \in (0,1)$ it is clear that

$$\begin{aligned}\mathbf{P}_{\mathbf{A,\,CI}} &> \mathbf{P_A}, \quad \mathbf{P}_{\mathbf{B,CI}} > \mathbf{P_B}, \qquad (37)\\ \mathbf{P}_{\mathbf{A,\,ICI}} &> \mathbf{P_A}, \quad \mathbf{P}_{\mathbf{B,ICI}} > \mathbf{P_B}, \qquad (38)\end{aligned}$$

where $\mathbf{P_x} > \mathbf{P}_y$ means $\mathbf{P_x} - \mathbf{P}_y$ is positive definite. (37-38) means that CI and ICI can be represented by naïve fusion with inflated covariance.

Since (35-36) have a minus operator that seems mathematically unstable, we will prove the positive definiteness (35-36). The equation (26) of the [44] is

$$(\mathbf{A}+\mathbf{UBV})^{-1} = \mathbf{A}^{-1} - \mathbf{A}^{-1}\,\mathbf{UBVA}^{-1}(\mathbf{I}+\mathbf{UBVA}^{-1})^{-1}. \qquad (39)$$

By substituting $\mathbf{A}=\mathbf{X},\ \mathbf{U}=\mathbf{Y},\ \mathbf{B}=\mathbf{V}=\mathbf{I}$, the inverse of a sum of matrices can be represented as

$$\begin{aligned}(\mathbf{X}+\mathbf{Y})^{-1} &= \mathbf{X}^{-1} - \mathbf{X}^{-1}\,\mathbf{YX}^{-1}(\mathbf{I}+\mathbf{YX}^{-1})^{-1} \\ &= \mathbf{X}^{-1} - (\mathbf{X}+\mathbf{XY}^{-1}\mathbf{X})^{-1}. \qquad (40)\end{aligned}$$

Substitute $\mathbf{X} = \mathbf{P_A},\ \mathbf{Y} = \frac{\omega}{1-\omega}\mathbf{P_A}\mathbf{P_B}^{-1}\mathbf{P_A}$ and remove subscript ICI from $\omega_{\mathbf{ICI}}$ for simplicity,

$$\begin{aligned}&(\mathbf{P_A} + \frac{\omega}{1-\omega}\mathbf{P_A}\ \mathbf{P_B}^{-1}\mathbf{P_A})^{-1} \\ &= \mathbf{P_A}^{-1} - (\mathbf{P_A} + \frac{1-\omega}{\omega}\mathbf{P}_B)^{-1} \\ &= \mathbf{P_A}^{-1} - \omega(\omega\mathbf{P_A} + (1-\omega)\mathbf{P}_B)^{-1} \\ &= \mathbf{P}_{\mathbf{A,ICI}}^{-1}. \qquad (41)\end{aligned}$$

Hence,

$$\mathbf{P}_{\mathbf{A,ICI}} = \mathbf{P_A} + \frac{\omega}{1-\omega}\mathbf{P_A}\mathbf{P_B}^{-1}\ \mathbf{P_A}. \qquad (42)$$

For the positive definite matrix $\mathbf{P_B}$, its inverse $\mathbf{P_B}^{-1}$ is also positive definite since eigenvalue $\mathbf{P_B}^{-1}$ is inverse to that of $\mathbf{P_B}$ which is also positive. Hence, for $\mathbf{x}^T\mathbf{P_A}\mathbf{x} > 0$ and $\mathbf{y}^T\,\mathbf{P_B}^{-1}\mathbf{y} > 0$, set $\mathbf{y} = \mathbf{P_A}\mathbf{x}$ then

$$\begin{aligned}\mathbf{x}^T\mathbf{P}_{\mathbf{A,ICI}}\mathbf{x} &= \mathbf{x}^T\mathbf{P_A}\mathbf{x} + \frac{\omega}{1-\omega}\,\mathbf{x}^T\mathbf{P_A}\mathbf{P_B}^{-1}\,\mathbf{P_A}\mathbf{x} \\ &= \mathbf{x}^T\mathbf{P_A}\mathbf{x} + \frac{\omega}{1-\omega}\ \mathbf{y}^T\mathbf{P_B}^{-1}\mathbf{y} \\ &> 0. \qquad (43)\end{aligned}$$

It means $\mathbf{P}_{\mathbf{A,ICI}}$ it is also positive definite and $\mathbf{P}_{\mathbf{B,ICI}}$ can be proved positive definite in the same way. To sum up, CI and ICI can be represented in naïve fusion with inflated covariance, which is also positive definite.

C. GENERALIZED INVERSE COVARIANCE INTERSECTION FOR MULTI TARGET TRACKING

As GCI is defined on the fusion of arbitrary pdfs, naïve fusion is defined as [38],

$$f(\mathbf{x}|\mathbf{Z}_a^k, \mathbf{Z}_b^k) \triangleq \frac{f_a(\,\mathbf{x}|\mathbf{Z}_a^k)f_b(\mathbf{x}|\mathbf{Z}_b^k)}{\int f_a(\,\mathbf{x}|\mathbf{Z}_a^k)f_b(\mathbf{x}|\,\mathbf{Z}_b^k)d\mathbf{x}}. \qquad (44)$$

Since GICI proposed in [35] includes convolution operation, it cannot be easily applied to the fusion of the finite sets.

Therefore, we will propose the GICI rule for the GM-CPHD by inflating the naïve fusion formula's covariance. The GM-naïve-CPHD formulas listed in (45-51) are the same from sections II-C, D except for erasing weight component of the CI.

$$f_{naive}(\mathbf{X}) = \frac{f_a(\mathbf{X})f_b(\mathbf{X})}{\int f_a(\ \mathbf{X})f_b(\mathbf{X})d\mathbf{X}} = \frac{n!\cdot p_a(n)p_b(n)\prod_{i=1}^{n} s_a(\mathbf{x}_i)\, s_b(\ \mathbf{x}_i)}{\sum_{m=0}^{\infty} p_a(m)p_b(m)\left(\int s_a(\mathbf{x})s_b(\ \mathbf{x})d\mathbf{x}\right)^m} = n!\cdot \bar{p}\,(n)\prod_{\mathbf{x}\in\mathbf{X}} \bar{s}(\ \mathbf{x}), \tag{45}$$

$$\bar{s}_{naive}(\mathbf{x}) = \frac{s_a(\mathbf{x})s_b(\mathbf{x})}{\int s_a(\mathbf{x})s_b(\mathbf{x})d\mathbf{x}}, \tag{46}$$

$$\bar{p}_{naive}(n) = \frac{p_a(n)p_b(n)\left(\int s_a(\mathbf{x})s_b(\ \mathbf{x})d\mathbf{x}\right)^n}{\sum_{m=0}^{\infty} p_a(m)p_b(m)\left(\int s_a(\ \mathbf{x})s_b(\mathbf{x})d\mathbf{x}\right)^m}. \tag{47}$$

Then, a closed-form solution is

$$\bar{s}_{naive}(\mathbf{x}) = \frac{s_a(\mathbf{x})s_b(\mathbf{x})}{\int s_a(\mathbf{x})s_b(\mathbf{x})d\mathbf{x}} = \frac{\sum_{i=1}^{N_G^a}\sum_{j=1}^{N_G^b}\alpha_{ij}^{(ab)}N(\hat{\mathbf{x}}_{ij}^{(ab)},\ \mathbf{P}_{ij}^{(ab)})}{\sum_{i=1}^{N_G^a}\sum_{j=1}^{N_G^b}\alpha_{ij}^{(ab)}}, \tag{48}$$

$$\mathbf{P}_{ij}^{(ab)} = \left[\left(\mathbf{P}_i^{(a)}\right)^{-1} + \left(\ \mathbf{P}_j^{(b)}\right)^{-1}\right]^{-1}, \tag{49}$$

$$\hat{\mathbf{x}}_{ij}^{(ab)} = \mathbf{P}_{ij}^{(ab)}\left[\left(\ \mathbf{P}_i^{(a)}\right)^{-1}\hat{\mathbf{x}}_i^{(a)} + \left(\mathbf{P}_j^{(b)}\right)^{-1}\hat{\mathbf{x}}_j^{b}\right], \tag{50}$$

$$\alpha_{ij}^{(ab)} = \left(\alpha_i^{(a)}\right)^{\omega}\left(\alpha_j^{(b)}\right)^{1-\omega} \cdot N\left(\hat{\mathbf{x}}_i^{(a)} - \hat{\mathbf{x}}_j^{(b)};\ 0,\ \mathbf{P}_i^{(a)} + \mathbf{P}_j^{(b)}\right). \tag{51}$$

D. COVARIANCE INFLATION FOR GICI

In the GM form of multi-object distribution (48-51), GICI can be proposed by substituting single object density covariance to inflated covariance using (35-36). The pseudocode for distributed GICI fusion is listed in Table 1. When extending naïve fusion to GICI, there is a question that inflating single object density is appropriate since the pdf in GM-CPHD is assumed to be a Gaussian mixture. The covariance of the Gaussian mixture can be represented as standard mixture merging [19],

$$\text{var}\,(s_a(\mathbf{x})) = \sum_{j=1}^{N_G^a}\alpha_j^{(a)}\left\{\mathbf{P}_j^{(a)} + \left(\hat{\mathbf{x}}_j^{(a)} - \sum_{k=1}^{N_G^a}\alpha_k\hat{\mathbf{x}}_k^{(a)}\right) \times \left(\hat{\mathbf{x}}_j^{(a)} - \sum_{k=1}^{N_G^a}\alpha_k\hat{\mathbf{x}}_k^{(a)}\right)^T\right\}, \tag{52}$$

TABLE 1. Pseudocode for the distributed GICI fusion.

Algorithm: Inflating covariance of the Gaussian mixtures based on naïve fusion

1: Obtain local GM-CPHD results by prediction, update, pruning & merging steps [45]
2: **for** $l = 1 : L$ (number of sensors)
3: Calculate ICI fusion weight ω_{ICI} by fast covariance intersection [42]
4: Substitute covariance of the single object densities $\mathbf{P}_i^{(a)}, \mathbf{P}_j^{(b)}$ (45) to

$$\begin{cases} \mathbf{P}_{i,\text{inf}}^{(a)} = \mathbf{P}_i^{(a)} + \dfrac{\omega_{\text{ICI}}}{1-\omega_{\text{ICI}}}\mathbf{P}_i^{(a)}\left(\mathbf{P}_j^{(b)}\right)^{-1}\mathbf{P}_i^{(a)} \\ \mathbf{P}_{j,\text{inf}}^{(b)} = \mathbf{P}_j^{(b)} + \dfrac{1-\omega_{\text{ICI}}}{\omega_{\text{ICI}}}\mathbf{P}_j^{(b)}\left(\mathbf{P}_i^{(a)}\right)^{-1}\mathbf{P}_j^{(b)} \end{cases}$$

5: Fuse inflated covariance based GM by naïve fusion (44-47)
6: Pruning & merging
7: **end for**
8: Estimate extraction [45]

Since $\mathbf{P}_j^{(a)}$ it is the error covariance of the state and $\left(\hat{\mathbf{x}}_j^{(a)} - \sum_{k=1}^{N_G^a}\alpha_k\hat{\mathbf{x}}_k^{(a)}\right)\left(\hat{\mathbf{x}}_j^{(a)} - \sum_{k=1}^{N_G^a}\alpha_k\hat{\mathbf{x}}_k^{(a)}\right)^T$ is the covariance generated by the state of the targets, the latter one is much bigger than the former one in the general case. It is the same context in the assumption on pseudo-Chernoff fusion (16,17), where the targets are well-separated. However, the coefficient becomes zero when fusing targets far apart, as shown in (51). We have to focus on fusing targets with a similar state, so inflating only a single object density is reasonable and proved in the simulation result.

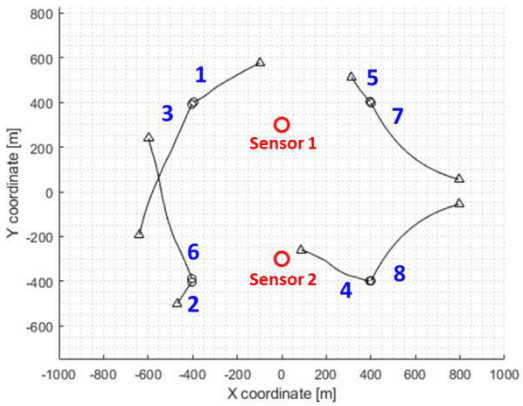

FIGURE 1. Ground truth in track 1 (8 targets) [8].

IV. SIMULATIONS

In the simulation, two-dimensional multi-target tracking examples with the most widely used linear Gaussian measurement model and a nonlinear measurement model are considered. The state is 2D-position and velocity $\mathbf{x}_k = [x_k\ \dot{x}_k\ y_k\ \dot{y}_k]^T$. In fig. 1, eight targets move from circle to triangle through solid black lines, which is the trajectory same as in [11]. The red circle is the position of the sensors, which are only relevant to the nonlinear measurement model. Fig.2 is another scenario that targets 1 and 2 encounters in the 40s, and targets 1 and 3 meet at the 80s. All the fusion weight

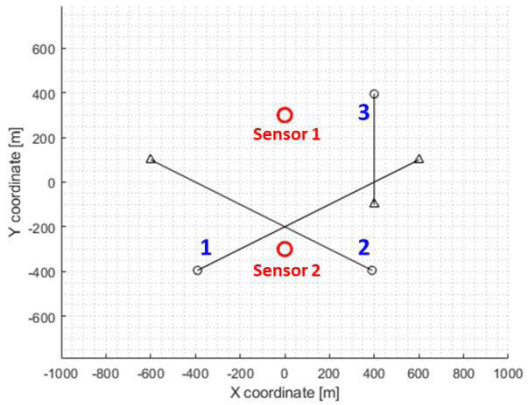

FIGURE 2. Ground truth in track 2 (3 targets with crossing).

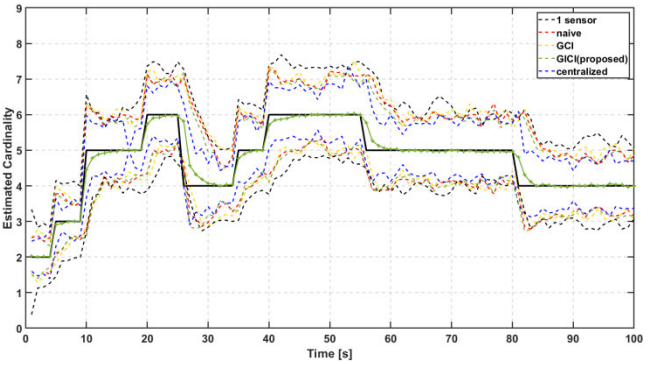

FIGURE 3. Estimated cardinality (linear case, track 1). The solid black line is the true cardinality, + is the mean cardinality (only GICI is plotted), and dot lines are 3σ the std of cardinality.

ω is obtained by fast covariance intersection [42], which just calculates traces of the matrices that do not increase the overall computational burden.

Total simulation time is 100 s with time interval 1s, and a GM-CPHD filter is used to track each sensor node's targets. Since it is evident that the performance is proportional to the number of sensors, we mainly analyze two sensor fusions. The system model is a constant velocity model,

$$\mathbf{x}_{k+1} = \mathbf{F}\mathbf{x}_k + \mathbf{w}_k, \quad \mathbf{w}_k \sim N(\mathbf{0}, \mathbf{Q}_k), \tag{53}$$

$$\mathbf{F} = \begin{bmatrix} \mathbf{I}_2 & T_s\mathbf{I}_2 \\ \mathbf{0}_2 & \mathbf{I}_2 \end{bmatrix},$$

$$\mathbf{Q}_k = \sigma_w^2 \begin{bmatrix} (T_s^3/3)\,\mathbf{I}_2 & (T_s^2/2)\mathbf{I}_2 \\ (T_s^2/2)\,\mathbf{I}_2 & T_s\,\mathbf{I}_2 \end{bmatrix}. \tag{54}$$

The probability of detection is 0.9, and the probability of survival is 0.99. The Poisson average rate of uniform clutter per scan is 5, and the birth densities are located at ($\pm$400m, $\pm$400m), as shown in the solid black circles in Fig. 1. All simulations are done with 100 Monte Carlo simulations, and ground truth is changed by process noise for each ensemble. The pruning threshold is 10^{-5}, and the merge threshold is 2.

In the following analysis, five implementations of GM-CPHD filter are compared: single sensor [45], naïve fusion, conventional GCI [22], proposed GICI, and centralized fusion [10]. Tracking performance is measured by optimal sub-pattern assignment (OSPA) distance [46]. The parameters for OSPA distance are set as cut-off parameter $c = 100$ and order parameter $p = 1$.

A. LINEAR GAUSSIAN MEASUREMENT MODEL

Firstly, a linear Gaussian measurement model is selected,

$$\mathbf{z}_k = \mathbf{H}_k\mathbf{x}_k + \mathbf{v}_k, \quad \mathbf{v}_k \sim N(\mathbf{0}, \mathbf{R}), \tag{55}$$

$$\mathbf{H}_k = [\mathbf{I}_2\ \mathbf{0}_2], \quad \mathbf{R} = \sigma_v^2\,\mathbf{I}_2, \tag{56}$$

where $\sigma_v = 10m$, and the model is irrelevant to the sensor position.

Fig. 3 is a cardinality estimate comparison for five methods. The solid black line is the true cardinality, + is the mean cardinality, and dot lines are 3σ standard deviations (std) of cardinality. Since it is hard to distinguish the mean cardinality performance with the cardinality estimate figure, only GICI is plotted representatively, and it will be compared in other OSPA error figures. Standard deviations are also hard to distinguish between 3 distributed fusions, but 1 sensor shows the biggest value, and centralized fusion shows the most negligible value as expected.

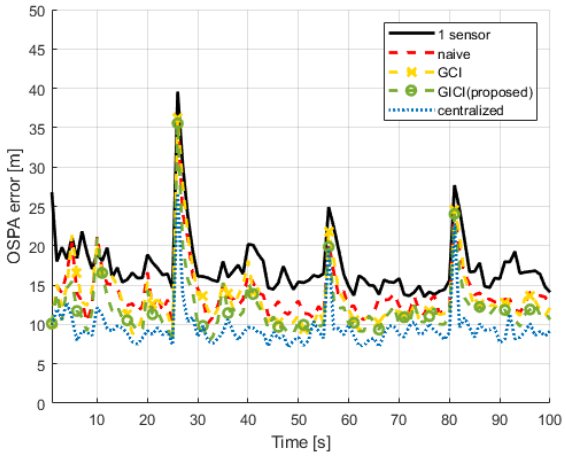

FIGURE 4. OSPA RMS (linear case, track 1).

Fig. 4 is the RMS OSPA error of the five implementations. OSPA error increases instantaneously at 25s, 55s, and 80s when the few targets are dead. Except for 1 sensor and centralized fusion, it shows good performance in the order of GICI, GCI, and naïve fusion. To see the difference clearly, the box plot of time-average OSPA errors is plotted together in fig. 5. Time-average OSPA means averaged 100 scans of OSPA in a single run, and the box plot is composed of 100 ensembles of the time-average OSPA. The performance of naïve fusion is effectively improved by inflating covariance as GICI.

Figs. 6 and 7 are simulation results for track 2. In track 2, two targets are meet exactly in the 40s and 80s. However, since the crossing targets' velocities are not the same at that time, significant performance degradation is not shown. Besides, there is a relatively bigger degradation on naïve and

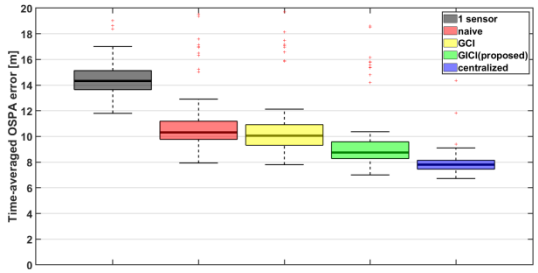

FIGURE 5. Box plot of time-average OSPA errors (linear case, track 1).

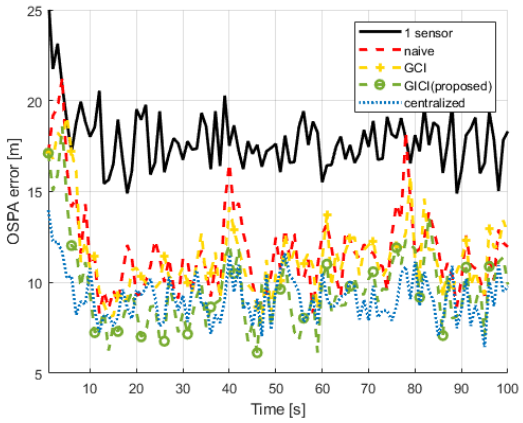

FIGURE 6. OSPA RMS (linear case, track 2).

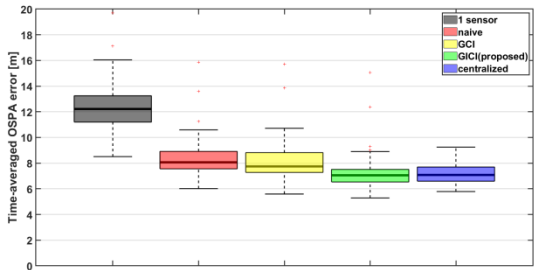

FIGURE 7. Box plot of time-average OSPA errors (linear case, track 2).

GCI than GICI and centralized fusion. In fig. 7, the box plot shows that GICI shows almost the same performance as the centralized fusion.

B. NONLINEAR MEASUREMENT MODEL

In nonlinear measurement model, range and bearing model is used,

$$\mathbf{z}_k = \begin{bmatrix} \sqrt{x_k^2 + y_k^2} \\ \arctan\left(\dfrac{y_k}{x_k}\right) \end{bmatrix} + \mathbf{v}_k, \tag{57}$$

where $\mathbf{v}_k \sim N(0, \mathbf{R}_k)$, $\mathbf{R}_k = diag\left(\sigma_r^2, \sigma_\theta^2\right)$ and $\sigma_r = 5m$, $\sigma_\theta = 1\,\text{deg}$.

Figs. 8 and 9 are results for track 1, and figs.10 and 11 are for track 2. As shown in the linear measurement case, the GCI and GICI showed better performance than the 1 sensor and naïve fusion. However, GCI and GICI show similar performance.

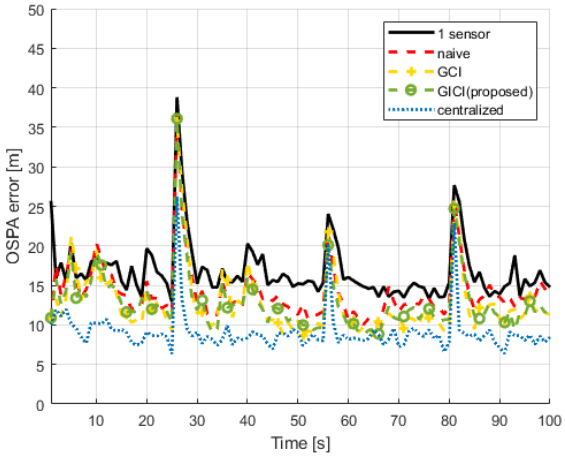

FIGURE 8. OSPA RMS (nonlinear case, track 1).

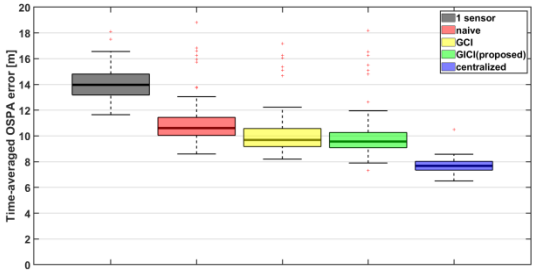

FIGURE 9. Box plot of time-average OSPA errors (nonlinear case, track 1).

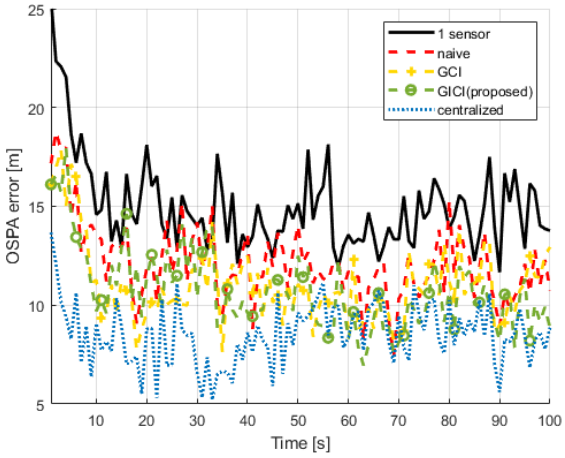

FIGURE 10. OSPA RMS (nonlinear case, track 2).

Also, additional simulations were performed using 5 snesors as shown in fig. 12. The result figs. 13 and 14 can be compared with the figs. 8 and 9, which are the results for the two sensors. As the number of sensors increases, centralized OSPA definitely decreases, whereas distributed fusion decreases the error less. In distributed fusions, the error peaks in figs. 8 and 13 are similar. It means that the cardinality error does not improve when the number of targets changes in the case of distributed fusion. In the section where the cardinality does not change, the localization error of fig. 13 is

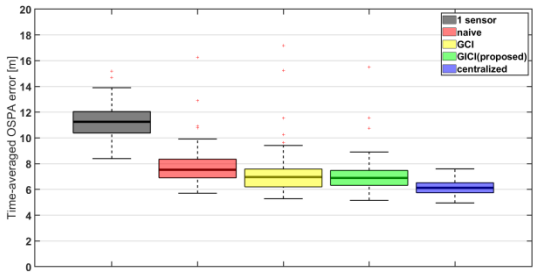

FIGURE 11. Box plot of time-average OSPA errors (nonlinear case, track2).

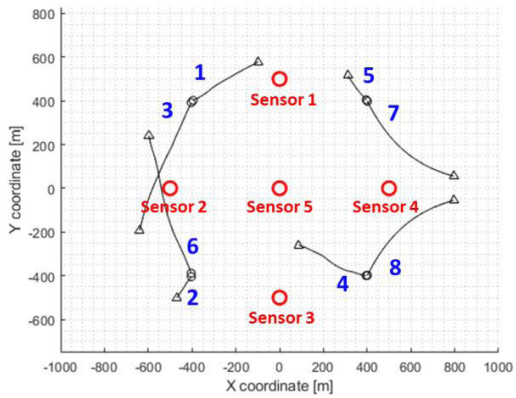

FIGURE 12. Ground truth in track 1 (8 targets, 5 sensors).

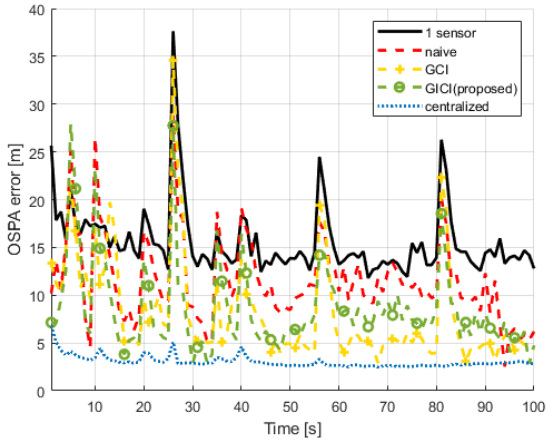

FIGURE 13. OSPA RMS (nonlinear case, track 1, 5 sensors).

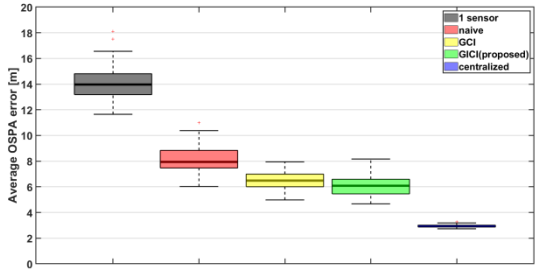

FIGURE 14. Box plot of time-average OSPA errors (nonlinear case, track 1, 5 sensors).

lower than that of fig. 8. However, the cardinality error is similar to the case of two sensors, so the performance is not significantly improved when viewed as a box plot average.

TABLE 2. Computational time of five GM-CPHD implementations (unit: s).

	1 sensor	Naïve	GCI	GICI (proposed)	Centralized
Linear, track 1	43.75	74.45	98.65	115.5	134.4
Nonlinear, track 1	43.75	73.55	97.15	113.9	136.4
Linear, track 2	34.70	49.19	70.60	83.40	94.43
Nonlinear, track 2	34.85	50.35	67.85	75.55	95.99
Average	39.26	61.89	83.56	97.06	115.3

On the other hand, as shown in fig. 14, it can be seen that even in 5 sensors, GICI has slightly superior performance over GCI.

Table 2 is the computational time for Monte Carlo 100times with Intel Core i7-9700K CPU 3.60GHz processor and 16GB RAM. It is assumed that the local nodes calculations are done in parallel in distributed fusion. The most time-consuming calculations are matrix inversion and determinant [23], and the proposed method have one more step to inflate the covariance than the naïve fusion.

V. CONCLUSION

In this research, we proposed the distributed GM-CPHD filter based on GICI and verified performance with multi-target tracking simulations. To apply the GICI fusion to MS-MT, the GICI formula was re-structured as naïve fusion with covariance inflation. For the positive definite covariance of the node, we proved the inflated covariance is also positive definite. The formula for RFS fusion was obtained in the same way as the previous GCI-based algorithms.

As a result, the proposed algorithm showed a smaller OSPA error than naïve fusion and conventional GCI-based algorithms. The performance improvement was shown clearly in the nonlinear measurement case and more robust when targets were crossing. Computational time becomes larger than the naïve fusion since the added step with matrix inversion is time-consuming. In future work, the GICI fusion will be applied to other RFS filters, such as MB filter.

REFERENCES

[1] R. P. Mahler, *Statistical Multisource-Multitarget Information Fusion*. Norwood, MA, USA: Artech House, 2007.
[2] R. P. S. Mahler, "Multitarget Bayes filtering via first-order multitarget moments," *IEEE Trans. Aerosp. Electron. Syst.*, vol. 39, no. 4, pp. 1152–1178, Oct. 2003.
[3] R. Mahler, "PHD filters of higher order in target number," *IEEE Trans. Aerosp. Electron. Syst.*, vol. 43, no. 99, pp. 1523–1543, Oct. 2007.
[4] B.-T. Vo and B.-N. Vo, "Labeled random finite sets and multi-object conjugate priors," *IEEE Trans. Signal Process.*, vol. 61, no. 13, pp. 3460–3475, Jul. 2013.
[5] B.-N. Vo, B.-T. Vo, and H. G. Hoang, "An efficient implementation of the generalized labeled multi-Bernoulli filter," *IEEE Trans. Signal Process.*, vol. 65, no. 8, pp. 1975–1987, Apr. 2017.
[6] W. J. Park and C. G. Park, "Road constrained labeled multi Bernoulli filter based on PDF truncation for multi-target tracking," in *Proc. IFAC World Congr.*, 2020, pp. 1–6.
[7] J. W. Choi and K. Samuel, "Robust UKF-IMM filter for tracking an off-road ground target," *Int. J. Control, Autom. Syst.*, vol. 17, no. 5, pp. 1149–1157, May 2019.
[8] W. Y. Choi, C. M. Kang, S.-H. Lee, and C. C. Chung, "Radar accuracy modeling and its application to object vehicle tracking," *Int. J. Control, Autom. Syst.*, vol. 18, no. 12, pp. 3146–3158, Dec. 2020.

[9] C. J. Lee, S. K. Park, and M. T. Lim, "Multi-target tracking and track management algorithm based on UFIR filter with imperfect detection probability," *Int. J. Control, Autom. Syst.*, vol. 17, no. 12, pp. 3021–3034, Dec. 2019.
[10] S. Nannuru, S. Blouin, M. Coates, and M. Rabbat, "Multisensor CPHD filter," *IEEE Trans. Aerosp. Electron. Syst.*, vol. 52, no. 4, pp. 1834–1854, Aug. 2016.
[11] A.-A. Saucan, M. J. Coates, and M. Rabbat, "A multisensor multi-Bernoulli filter," *IEEE Trans. Signal Process.*, vol. 65, no. 20, pp. 5495–5509, Oct. 2017.
[12] B.-N. Vo, B.-T. Vo, and M. Beard, "Multi-sensor multi-object tracking with the generalized labeled multi-Bernoulli filter," *IEEE Trans. Signal Process.*, vol. 67, no. 23, pp. 5952–5967, Dec. 2019.
[13] T. Li, X. Wang, Y. Liang, and Q. Pan, "On arithmetic average fusion and its application for distributed multi-Bernoulli multitarget tracking," *IEEE Trans. Signal Process.*, vol. 68, pp. 2883–2896, 2020.
[14] M. Frohle, K. Granstrom, and H. Wymeersch, "Decentralized Poisson multi-Bernoulli filtering for vehicle tracking," *IEEE Access*, vol. 8, pp. 126414–126427, 2020.
[15] Y. Yu and Y. Liang, "Distributed multitarget tracking based on diffusion strategies over sensor networks," *IEEE Access*, vol. 7, pp. 129802–129814, 2019.
[16] C. Hu, Z. Meng, G. Qu, H. S. Shin, and A. Tsourdos, "Distributed cooperative path planning for tracking ground moving target by multiple fixed-wing UAVs via DMPC-GVD in urban environment," *Int. J. Control, Autom. Syst.*, vol. 19, no. 2, pp. 823–836, 2021.
[17] K. Da, T. Li, Y. Zhu, H. Fan, and Q. Fu, "Recent advances in multisensor multitarget tracking using random finite set," *Frontiers Inf. Technol. Electron. Eng.*, vol. 22, no. 1, pp. 5–24, Jan. 2021.
[18] T. Li, Z. Liu, and Q. Pan, "Distributed Bernoulli filtering for target detection and tracking based on arithmetic average fusion," *IEEE Signal Process. Lett.*, vol. 26, no. 12, pp. 1812–1816, Dec. 2019.
[19] T. Li, J. M. Corchado, and S. Sun, "Partial consensus and conservative fusion of Gaussian mixtures for distributed PHD fusion," *IEEE Trans. Aerosp. Electron. Syst.*, vol. 55, no. 5, pp. 2150–2163, Oct. 2019.
[20] T. Li, H. Fan, J. García, and J. M. Corchado, "Second-order statistics analysis and comparison between arithmetic and geometric average fusion: Application to multi-sensor target tracking," *Inf. Fusion*, vol. 51, pp. 233–243, Nov. 2019.
[21] W. Wu, H. Sun, Z. Huang, J. Xiong, M. Zheng, and C. Chen, "Multi-GMTI fusion for Doppler blind zone suppression using PHD fusion," *Signal Process.*, vol. 183, pp. 1–13, Jun. 2021.
[22] G. Battistelli, L. Chisci, C. Fantacci, A. Farina, and A. Graziano, "Consensus CPHD filter for distributed multitarget tracking," *IEEE J. Sel. Topics Signal Process.*, vol. 7, no. 3, pp. 508–520, Jun. 2013.
[23] G. Lai, S. Li, W. Yi, G. Battistelli, L. Chisci, and L. Kong, "Computationally efficient CPHD fusion based on generalized covariance intersection," in *Proc. IEEE Radar Conf. (RadarConf)*, Apr. 2019, pp. 1–6.
[24] B. Wang, W. Yi, R. Hoseinnezhad, S. Li, L. Kong, and X. Yang, "Distributed fusion with multi-Bernoulli filter based on generalized covariance intersection," *IEEE Trans. Signal Process.*, vol. 65, no. 1, pp. 242–255, Jan. 2017.
[25] W. Yi, S. Li, B. Wang, R. Hoseinnezhad, and L. Kong, "Computationally efficient distributed multi-sensor fusion with multi-Bernoulli filter," *IEEE Trans. Signal Process.*, vol. 68, pp. 241–256, 2020.
[26] R. P. S. Mahler, "Optimal/robust distributed data fusion: A unified approach," *Proc. SPIE*, vol. 4052, pp. 128–138, Aug. 2000.
[27] D. Clark, S. Julier, R. Mahler, and B. Ristic, "Robust multi-object sensor fusion with unknown correlations," in *Proc. Sensor Signal Process. Defence (SSPD)*, 2010, pp. 1–5.
[28] J. K. Uhlmann, "General data fusion for estimates with unknown cross covariances," *Proc. SPIE*, vol. 2755, pp. 536–547, Jun. 1996.
[29] S. J. Julier, "An empirical study into the use of Chernoff information for robust, distributed fusion of Gaussian mixture models," in *Proc. 9th Int. Conf. Inf. Fusion (FUSION)*, Jul. 2006, pp. 1–8.
[30] M. Gunay, U. Orguner, and M. Demirekler, "Chernoff fusion of Gaussian mixtures based on sigma-point approximation," *IEEE Trans. Aerosp. Electron. Syst.*, vol. 52, no. 6, pp. 2732–2746, Dec. 2016.
[31] J. Sijs and M. Lazar, "State fusion with unknown correlation: Ellipsoidal intersection," *Automatica*, vol. 48, no. 8, pp. 1874–1878, Aug. 2012.
[32] B. Noack, J. Sijs, M. Reinhardt, and U. D. Hanebeck, "Decentralized data fusion with inverse covariance intersection," *Automatica*, vol. 79, pp. 35–41, May 2017.
[33] C. H. Kang, S. Y. Kim, and J. W. Song, "Data fusion with inverse covariance intersection for prior covariance estimation of the particle flow filter," *IEEE Access*, vol. 8, pp. 221203–221213, 2020.
[34] H. Tang, H. Liu, B. Liu, X. Shen, and P. K. Varshney, "Some results on generalized ellipsoid intersection fusion," in *Proc. 22nd Int. Conf. Inf. Fusion (FUSION)*, 2019, pp. 7–12.
[35] B. Noack, U. Orguner, and U. D. Hanebeck, "Nonlinear decentralized data fusion with generalized inverse covariance intersection," in *Proc. IEEE 22nd Int. Conf. Inf. Fusion*, Jul. 2019, pp. 1–7.
[36] N. A. Carlson, "Federated square root filter for decentralized parallel processors," *IEEE Trans. Aerosp. Electron. Syst.*, vol. 26, no. 3, pp. 517–525, May 1990.
[37] S. Sun, H. Lin, J. Ma, and X. Li, "Multi-sensor distributed fusion estimation with applications in networked systems: A review paper," *Inf. Fusion*, vol. 38, pp. 122–134, Nov. 2017.
[38] K. Chang, C.-Y. Chong, and S. Mori, "Analytical and computational evaluation of scalable distributed fusion algorithms," *IEEE Trans. Aerosp. Electron. Syst.*, vol. 46, no. 4, pp. 2022–2034, Oct. 2010.
[39] M. Liggins, D. Hall, and J. Llinas, *Handbook of Multisensor Data Fusion: Theory and Practice*, 2nd ed. Boca Raton, FL, USA: CRC Press, 2008.
[40] W. Niehsen, "Information fusion based on fast covariance intersection filtering," in *Proc. 5th Int. Conf. Inf. Fusion (FUSION)*, 2002, pp. 901–904.
[41] D. Fränken and A. Hüpper, "Improved fast covariance intersection for distributed data fusion," in *Proc. 7th Int. Conf. Inf. Fusion (FUSION)*, vol. 1, 2005, pp. 290–297.
[42] J. Cong, Y. Li, G. Qi, and A. Sheng, "An order insensitive sequential fast covariance intersection fusion algorithm," *Inf. Sci.*, vols. 367–368, pp. 28–40, Nov. 2016.
[43] U. Orguner, "Approximate analytical solutions for the weight optimization problems of CI and ICI," in *Proc. Sensor Data Fusion, Trends, Solutions, Appl. (SDF)*, Oct. 2017, pp. 1–6.
[44] H. V. Henderson and S. R. Searle, "On deriving the inverse of a sum of matrices," *SIAM Rev.*, vol. 23, no. 1, pp. 53–60, Jan. 1981.
[45] B.-T. Vo, B.-N. Vo, and A. Cantoni, "Analytic implementations of the cardinalized probability hypothesis density filter," *IEEE Trans. Signal Process.*, vol. 55, no. 7, pp. 3553–3567, Jul. 2007.
[46] D. Schuhmacher, B.-T. Vo, and B.-N. Vo, "A consistent metric for performance evaluation of multi-object filters," *IEEE Trans. Signal Process.*, vol. 56, no. 8, pp. 3447–3457, Aug. 2008.

WOO JUNG PARK received the B.S. degree in mechanical and aerospace engineering and the M.S. degree in interdisciplinary program of bioengineering from Seoul National University, South Korea, in 2014 and 2016, respectively, where he is currently pursuing the Ph.D. degree with the Department of Mechanical and Aerospace Engineering. His current research interests include target tracking and land vehicle navigation.

CHAN GOOK PARK (Member, IEEE) received the B.S., M.S., and Ph.D. degrees in control and instrumentation engineering from Seoul National University, Seoul, South Korea, in 1985, 1987, and 1993, respectively.

He was as a Postdoctoral Fellow with Prof. J. L. Speyer about peak seeking control for formation flight with the University of California at Los Angeles, Los Angeles, CA, USA, in 1998. From 1994 to 2003, he was an Associate Professor with Kwangwoon University, Seoul. In 2003, he joined as a Faculty Member with the Department of Mechanical and Aerospace Engineering, National University, Seoul, where he is currently a Professor. In 2009, he was a Visiting Scholar with the Department of Aerospace Engineering, Georgia Institute of Technology, Atlanta, GA, USA. His current research interests include advanced filtering techniques, high precision inertial navigation systems (INS), visual-inertial odometry (VIO), INS/GNSS/IBN integration, and smartphone-based/foot-mounted pedestrian dead reckoning (PDR) systems. He served as the Chair for IEEE AES Korea Chapter, until 2009.